# EEG microstate sequences in healthy humans at rest reveal scale-free dynamics

Dimitri Van De Ville[a,b,1], Juliane Britz[c], and Christoph M. Michel[c,d]

[a]Department of Radiology and Medical Informatics, University of Geneva, 1211 Geneva, Switzerland; [b]Institute of Bioengineering, École Polytechnique Fédérale de Lausanne, 1015 Lausanne, Switzerland; [c]Department of Fundamental Neuroscience, University of Geneva, 1211 Geneva, Switzerland; and [d]Department of Neurology, University of Geneva, 1211 Geneva, Switzerland

Edited* by Nikos K. Logothetis, Max Planck Institute for Biological Cybernetics, Tuebingen, Germany, and approved September 7, 2010 (received for review June 14, 2010)

**Recent findings identified electroencephalography (EEG) microstates as the electrophysiological correlates of fMRI resting-state networks. Microstates are defined as short periods (100 ms) during which the EEG scalp topography remains quasi-stable; that is, the global topography is fixed but strength might vary and polarity invert. Microstates represent the subsecond coherent activation within global functional brain networks. Surprisingly, these rapidly changing EEG microstates correlate significantly with activity in fMRI resting-state networks after convolution with the hemodynamic response function that constitutes a strong temporal smoothing filter. We postulate here that microstate sequences should reveal scale-free, self-similar dynamics to explain this remarkable effect and thus that microstate time series show dependencies over long time ranges. To that aim, we deploy wavelet-based fractal analysis that allows determining scale-free behavior. We find strong statistical evidence that microstate sequences are scale free over six dyadic scales covering the 256-ms to 16-s range. The degree of long-range dependency is maintained when shuffling the local microstate labels but becomes indistinguishable from white noise when equalizing microstate durations, which indicates that temporal dynamics are their key characteristic. These results advance the understanding of temporal dynamics of brain-scale neuronal network models such as the global workspace model. Whereas microstates can be considered the "atoms of thoughts," the shortest constituting elements of cognition, they carry a dynamic signature that is reminiscent at characteristic timescales up to multiple seconds. The scale-free dynamics of the microstates might be the basis for the rapid reorganization and adaptation of the functional networks of the brain.**

critical state | microstates | resting-state networks | self-similar processes | wavelet fractal analysis

The human brain is intrinsically organized into interconnected neuronal clusters that form large-scale neurocognitive networks (1, 2). These networks have to dynamically and rapidly reorganize and coordinate on subsecond temporal scales to allow the execution of mental processes in a timely fashion (3, 4). Precise timing is crucial for the government of the continuous information flow from multiple sources to ensure perception, cognition, and action and ultimately consciousness. The anatomical architecture of several large-scale networks is well known and has been studied with different methods ranging from tracer studies to resting-state fMRI (5, 6). However, much less is known about their underlying temporal dynamics.

Multichannel electroencephalography (EEG) is a key method to access real-time information about the function of large-scale neuronal networks with high temporal resolution. Traditionally, spontaneous EEG analysis relies mainly on the power variation in different frequency bands at a subset of electrodes; however, observing this variation inherently sacrifices temporal accuracy due to the time-frequency uncertainty principle. To account for short-lasting fluctuations of neuronal activity, analysis methods in the time domain are required. Lehmann and coworkers proposed to consider the temporal evolution of the topography of the scalp electric field, because it represents the sum of all momentarily active sources in the brain, irrespective of their frequency. This way, one obtains a global measure of momentary brain activity with high temporal resolution. The topography does not change randomly and continuously over time, but remains stable for ~80–120 ms; these periods of quasi-stability are termed "EEG microstates" (7, 8). Cognition (9) and perception (10, 11) have been found to vary as a direct function of the prestimulus microstate, and microstates can characterize qualitative aspects of spontaneous thoughts (12, 13). This result indicates that they index different types of mental processes. Surprisingly, only four different microstates are consistently observed at rest (14). They reproduce well across subjects and can be identified across the entire life span (15), indicating that they might be mediated by predetermined anatomical connections. Alterations of microstates have been reported in schizophrenia (16, 17), depression (18), and Alzheimer's disease (19, 20) and as a function of drug administration and hypnosis (21–23).

Recent work (24, 25) revealed a link between the rapid changes in the time courses of EEG microstate sequences on the one hand and slow coherent changes in the blood oxygen-level–dependent (BOLD) signal obtained with fMRI during rest on the other hand. More precisely, we identified the four prototypical EEG microstates during rest that each could explain one large-scale resting-state network (RSN) obtained from BOLD fMRI (25). This finding indicates that the EEG microstates are strong candidates for the electrophysiological signatures of these RSNs. At first sight, this link is surprising due to the different timescales at which both signals are meaningful, i.e., 50–100 ms for EEG microstates vs. 5–10 s for BOLD fMRI. The connection between EEG microstates and fMRI RSNs was established by convolving the time courses of the occurrence of the different EEG microstates with the hemodynamic response function (HRF) and then using these as regressors in a general linear model for conventional fMRI analysis, as illustrated in Fig. 1*A*. Because the HRF acts as a strong temporal smoothing filter on the rapid EEG-based signal, it is remarkable that statistically significant correlations can be found. The fact that this smoothing did not remove any information-carrying signal from the microstate sequence and that furthermore the original microstate sequences and the regressors show the same relative behavior at temporal scales about two orders of magnitude apart suggests that the time courses of the EEG microstates are scale invariant. The working hypothesis of this paper is that the microstate dynamics have fractal properties. We investigated whether they show statistically self-similar, scale-free properties over a large time range, which preserves their information after smoothing with the hemodynamic filter as shown in Fig. 1*B*.

Several complex structures in nature manifest fractal behavior: Statistically the object looks the same on a wide range of observation scales. Fractals are most commonly associated with 2D

Author contributions: D.V.D.V., J.B., and C.M.M. designed research; D.V.D.V., J.B., and C.M.M. performed research; D.V.D.V. contributed new reagents/analytic tools; D.V.D.V. and J.B. analyzed data; and D.V.D.V., J.B., and C.M.M. wrote the paper.

The authors declare no conflict of interest.

*This Direct Submission article had a prearranged editor.

[1]To whom correspondence should be addressed. E-mail: dimitri.vandeville@epfl.ch.

This article contains supporting information online at www.pnas.org/lookup/suppl/doi:10.1073/pnas.1007841107/-/DCSupplemental.

NEUROSCIENCE

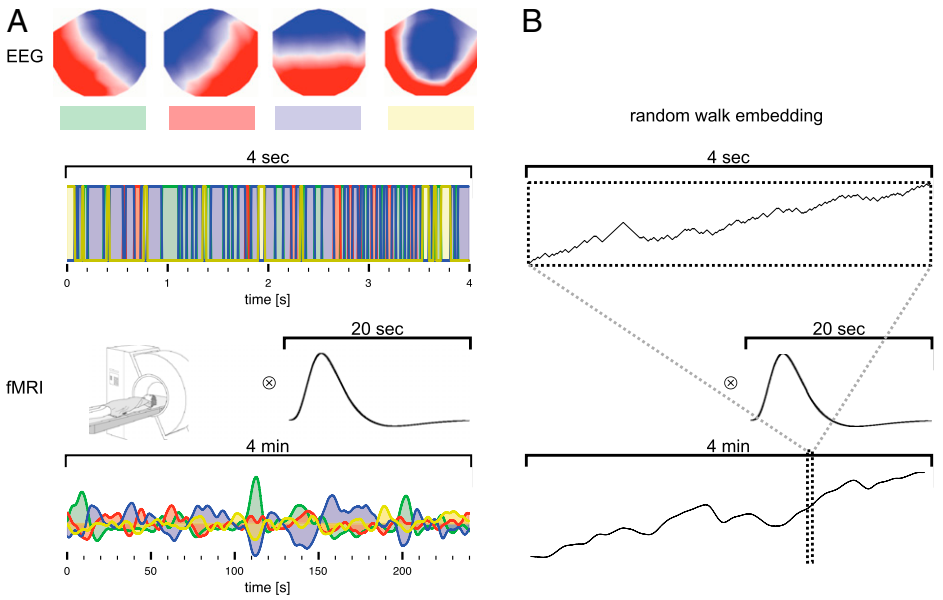


**Fig. 1.** (*A*) Illustration of the link between EEG microstates and their manifestation at the fMRI level. Our recent work (25) showed that after convolution of the EEG microstate sequences with the hemodynamic response function, which introduces a strong temporal smoothing, the resulting signals correlate significantly with large-scale RSNs. (*B*) To investigate the intriguing link between microstate sequences at the EEG and fMRI level, we study the fractal properties of their random walk embedding. Scale-free dynamics or statistical self-similarity is reflected by the same behavior of the random walk at various timescales.

artificial or natural geometric objects like Mandelbrot sets or fern leaves. One-dimensional time courses can also show self-similarity, which has often been associated with a critical state due to the lack of a characteristic scale. Quantitative assessment of fractal behavior was intensively studied in the 1980s (26). The most notable examples are distinct fractal properties of coding and noncoding parts of human DNA sequences (27) and changes of heartbeat dynamics related to pathological conditions (28, 29). Monofractal behavior can be characterized by a single parameter, the Hurst exponent, which is a measure of the extent of long-range dependency. Clearly, pure monofractality imposes a strong constraint, which is why experimental data are often explained by multifractal models at the expense of additional parameters, the so-called higher-degree cumulants.

The investigation of scale-free organization in the brain has been a long-standing research topic, related both to anatomy (30, 31) and to function (32–36). Many studies have characterized the fractal properties of local aspects of EEG temporal dynamics, namely of amplitude modulations at single electrodes (37–40); these properties have been linked to cognitive tasks (41), sleep (42–44), and clinical conditions such as epilepsy (45, 46), Alzheimer's disease (47, 48), mania (49), dementia (50), and schizophrenia (51). Whereas these studies indicate that the fractal characterization of electric potential time series can be a useful measure of local brain activity, they cannot be related to the temporal properties of global brain networks. In contrast, the EEG microstates are measures of the global brain activity and are directly correlated with the fMRI RSNs. Therefore, fractal behavior of microstate alterations would directly demonstrate scale-free properties of the temporal dynamics of large-scale neuronal networks.

To this end we here investigate in detail whether the time series of the EEG scalp topography—the sequence of the four dominant EEG microstates—reveal scale-free dynamics. Previous research has shown short-range dependency in the time series of EEG microstates (52) and their alteration in schizophrenia (53), but their long-range dependency and potentially scale-free dynamics have never been investigated. To that aim, we deploy a wavelet analysis framework that is able to distinguish between mono- and multifractal behavior. In the light of the previous connection with fMRI RSNs, we analyze EEG recorded inside the MR scanner. Cleaning the EEG recorded inside the MR scanner involves several filtering steps, which could in principle induce long-range dependency. To rule this out, we investigate the effects of filtering on EEG recorded outside the scanner for both the original and the temporally permuted data. We then study how microstate sequence modifications alter the dynamics to establish the key microstate characteristics. Finally, we discuss the implications of our results for temporal dynamics of neuronal models.

## Results

Fig. 2 depicts the steps of the fractal analysis. First, we segment the EEG into microstate sequences (Fig. 2*A*). Second, we split the sequences of microstate labels (i.e., the time series of their occurrence) into the three possible bipartitions (1, 2 vs. 3, 4; 1, 3 vs. 2, 4; and 1, 4 vs. 2, 3; Fig. 2*B*). Third, we construct three random walkers corresponding to these bipartitions: The walker steps either up (+1) or down (−1), depending on the partition label. In other words, we generate the cumulative sum of the bipartition labels (Fig. 2*C*). Our analysis aims at characterizing the type of correlations that occur in such a random walk, i.e., short range (as in Markov models) vs. long range (as in scale-free phenomena). For this evaluation, we examine the displacement $X(n)$ of the random walk after $n$ steps. In Fig. 2*D*, the random walk is observed at various scales showing similar time courses. Fourth, we analyze the random walk signal with the wavelet transform (Fig. 2*E*), which is the natural tool to study fractality due to the intrinsic scale invariance of the wavelet basis functions and its ability to deal efficiently with nonstationary signals; here, we use orthogonal Daubechies wavelets with five vanishing moments (54). The wavelet coefficient at dyadic scale $j$ and position $k$ reflects the imprint of the random walk embedding on the dilated and shifted wavelet function $\psi\,(t/2^j-k)$ and can be computed efficiently using the filterbank algorithm (55). One reminiscent feature of scale-free behavior is the linear relationship (in the log scale) between the energy of the wavelet coefficients and scale $j$, which can be plotted in the log-scaling diagram (Fig. 2*F*). Finally, on the basis of the fitting region in the log-scaling diagram, that is, where the power law holds, the scaling spectrum can be determined (Fig. 2*G*) to extract the fractal signature and various key parameters, in particular the Hurst exponent for monofractal behavior (characterized by the slope of a linear scaling spectrum) and higher-degree cumulants for multifractal behavior.

We found that all random walk embeddings associated with EEG microstate sequences show clear power laws over six dyadic scales that cover two orders of magnitude between 256 ms and 16 s. Fractal analysis is performed on this fitting region (see Fig. S1 for the group-level log-scaling diagrams). The lower bound of the fitting region can be explained by the lowest scale at which microstate *alterations* become "visible" to the analyzing wavelet function. The choice of the bipartitioning of the microstate labels did not yield any statistically significant changes in the outcome of the fractal parameters (Fig. S2).

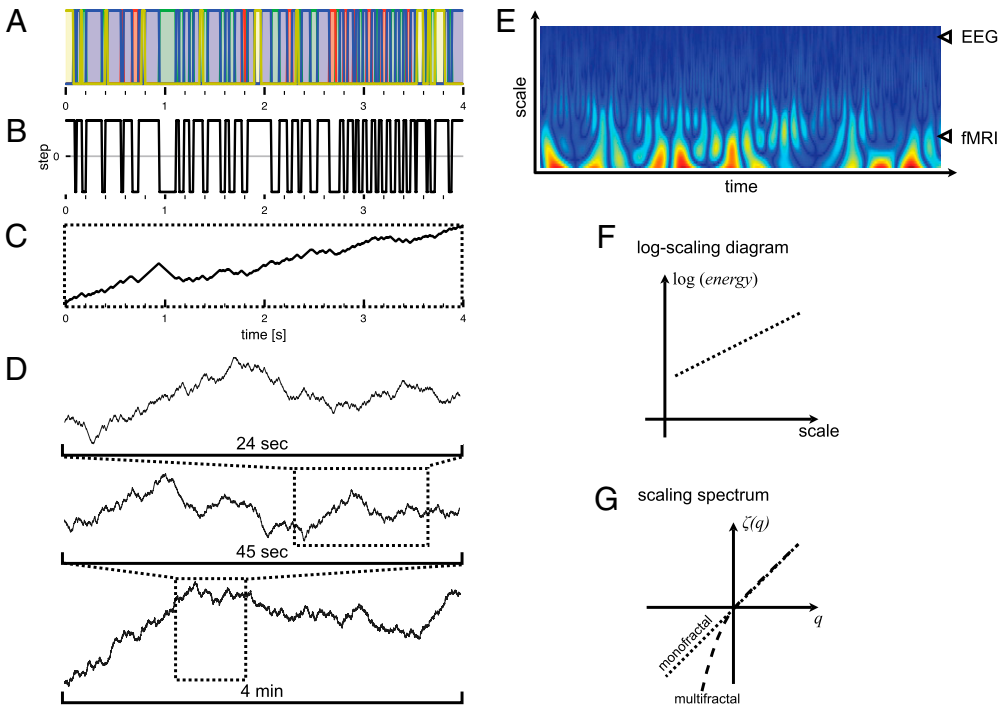


**Fig. 2.** Illustration of the wavelet fractal analysis. (*A*) The microstate sequence over a short period. (*B*) Microstates are partitioned into two classes and associated with a positive and a negative step, respectively. (*C*) Random walk embedding by the cumulative sum of *B* until each time point. (*D*) The complete random walk embedding of a resting-state recording at various timescales. Similar time courses are obtained when observing the signal at different scales. (*E*) Color-coded wavelet transform of the random walk embedding. Brighter colors indicate larger magnitude of the wavelet coefficients. The *x* axis represents time (3 min), and the *y* axis specifies scale (from ~256 ms to 16 s, top to bottom). The pointers indicate the approximate timescales of EEG and fMRI. The evolution of several measures of the wavelet coefficients over scale (e.g., the structure function of Eq. **2**) provides us with a comprehensive way to study fractal behavior. For illustration purposes, the continuous wavelet transform is shown (scale varies continuously); the fractal wavelet analysis needs only discrete dyadic scales. (*F*) The power-law behavior of the wavelet coefficients is verified using the log-scaling diagram. (*G*) The scaling spectrum allows us to identify the signature of mono- and multifractality.

Fig. 3 shows the Hurst exponent $H$ for the individual subjects for the data recorded inside the scanner (black bars). We found scale-free behavior with long-range dependency ($H > 0.5, P < 0.05$) for every individual. To confirm the monofractality of the microstate sequences, we also analyzed additional fractal parameters (higher-degree cumulants $c_2$ and $c_3$) that allow departures from "pure" self-similarity according to the multifractal model. This analysis confirmed that the microstate dynamics are indeed monofractal: The results and the group-level statistics are listed in Table S1. Furthermore, the scaling spectra at the group level reflect a remarkably accurate linear behavior, a clear indication for monofractality; they are shown in Fig. S3. In addition, Fig. 3 shows the Hurst exponent for the individual subjects for the data recorded outside the scanner as a function of both filtering and temporal permutation. We found comparable measures of monofractality for the original nonfiltered and filtered data ($H > 0.5, P < 0.05$; Fig. 3, blue bars). However, long-range dependency is completely eliminated after temporal permutation of the original EEG data. The corresponding microstate sequences behave like white noise for the permuted nonfiltered and filtered data ($H = 0.5$; Fig. 3, green bars). An overview of the fractal parameters and statistical analysis is listed in Table S1.

For the data recorded inside the scanner, we then altered the microstate sequence to investigate the relative importance of the sequence of microstate labels and durations on their monofractal signature. First, we randomly shuffled the microstate labels while preserving the duration. The resulting sequences are still significantly monofractal with no significant change in long-range dependency (Fig. 4, bars with light shading) for every individual; the group statistics are summarized in Table S2. This result indicates that the sequence of labels is not crucial for long-range dependency. Second, we preserved the original microstate sequence while equalizing the microstate duration to investigate the effect of timing. The resulting sequences are indistinguishable from white noise ($H = 0.5$; Fig. 4, open bars) for every individual; the group statistics are summarized in Table S2. This result indicates that the correct timing is the crucial parameter for the monofractal signature.

## Discussion

We investigated the scale-free dynamics of a measure of global brain state, i.e., time courses of EEG microstates. This investigation was motivated by the recent connection made between rapid EEG microstates and the slow fMRI RSNs. They are two global measures of overall brain activity that can be assessed on very fast and very slow temporal scales, respectively (25). We found strong statistical evidence of monofractal behavior of the EEG microstate alterations spanning six dyadic scales or two orders of magnitude (256 ms to 16 s), i.e., spanning the timescales characteristic of EEG microstate changes and fMRI BOLD oscillations. This finding provides the explanation for how information that can be observed at such different timescales is intertwined. Monofractal behavior also implies nonstationarity, which is a well-known feature of EEG data (56). Recent work relating RSNs observed by magnetoencephalography (MEG) and BOLD fMRI suggested coexistence of nonstationary (MEG) and stationary (fMRI) processes on

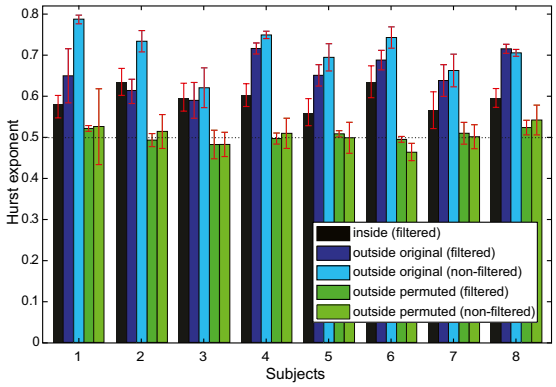


**Fig. 3.** Hurst exponent for the different subjects, recorded inside and outside the scanner, for the microstate sequences based on the original and permuted EEG data, with and without filtering. The error bars indicate the SD of the estimate over sessions and possible bipartitions of the microstates.

similar anatomical substrates (57). However, the present findings show that scale-free dynamics cover timescales from (fast) EEG to (slow) fMRI, suggesting that the information at both scales reflects the same (nonstationary) underlying physiological process. This result also extends the finding that synchronization metrics during rest between different channels in MEG and between brain regions in fMRI show power law scaling behavior (62).

We could rule out that the long-range dependency is an artifact of temporal filtering. We actually found stronger long-range dependency for nonfiltered than for filtered data. We further showed that temporal permutation removes all long-range dependency from the data. Finally, filtering of the permuted data does not reinstate long-range dependency. This result shows that filtering in the temporal domain does not induce long-range dependency in the microstate sequence. On the contrary, temporal filtering reduces rather than induces the long-range dependency. We further investigated whether the local sequence or the timing of the microstates is crucial for their monofractal signature and performed fractal analysis of modified microstate sequences. The shuffled microstate labels (with preserved durations) maintained monofractal behavior ($H > 0.5, P < 0.05$) that was not significantly different from the original sequence. The duration-equalized sequence (with preserved microstate labels) behaved like white noise. On the basis of these results, we state that microstate duration is the most crucial constitutive parameter; without this parameter, long-range dependency is absent. This result is perfectly in line with the notion that precise timing is crucial for the government of the constant information flow the brain has to deal with at every instant to enable perception, cognition, and ultimately consciousness. This result also confirms previous studies about microstate changes in schizophrenia that mainly affect the microstates' duration (53). It also corroborates the fact that modeling microstate syntax needs to go beyond short-range interactions such as modeled by $n$-step Markov chains (52).

Scale-free dynamics of microstate sequences imply nonstationarity of the underlying brain activity. Indeed, spontaneous EEG makes an ideal candidate to observe this type of phenomenon; any kind of averaging such as for evoked potentials would destroy the fractal structure of the data. Moreover, self-similarity is also closely related to the notion of universality and self-organized criticality; i.e., scale-free dynamics arise only when neuronal systems reach a critical point (33, 58). An efficient quantification of the critical state could also contribute to characterizing phase transitions related to neurological conditions (59) and as an essential prerequisite for learning (60), inspired by modification of functional connectivity as observed by fMRI (61). Moreover, this type of analysis opens a multitude of possibilities for future research based on the fractal signature of microstate sequences.

One characteristic feature of EEG microstates is the rapid transition from one scalp field topography into another, leading to the hypothesis that they constitute the "basic building blocks of cognition" or "atoms of thought" that underlie spontaneous conscious cognitive activity (63, 64). Moreover, during rest, four dominant microstates are systematically observed as confirmed by a comprehensive study of 496 subjects (15). This hypothesis also fits well with the concept of the neuronal workspace model of consciousness (65, 66), a link that was recently proposed (67). The spontaneous fluctuations of electrical activity characterized by microstates provide a compelling explanation for top–down processing as opposed to the classical bottom–up view of brain function. The observed fractal behavior of microstates sheds a unique light on intrinsic temporal dynamics of the neuronal workspace model, which have remained unexplored. Indeed, scale-free dynamics provide an organizing mechanism (68) for a complex system like the brain to operate far from homeostatis and to flexibly govern the incessant information flow from multiple sources—being close to the critical state of the system enables it to reconfigure with a high degree of responsiveness.

In addition, fractal properties of synchronized activity between brain regions (69) have been at the basis of "operational modules" in the sense (70) that they are embedded at various temporal scales; i.e., modules covering large cortical networks are supposedly active during short durations whereas small modules are associated with small local networks (involved in more complex tasks). However, instead of these modules being active at different frequency oscillations, functional microstates and their fractal organization turn them into ideal candidates for a universal representation that is reminiscent of a wide range of temporal scales.

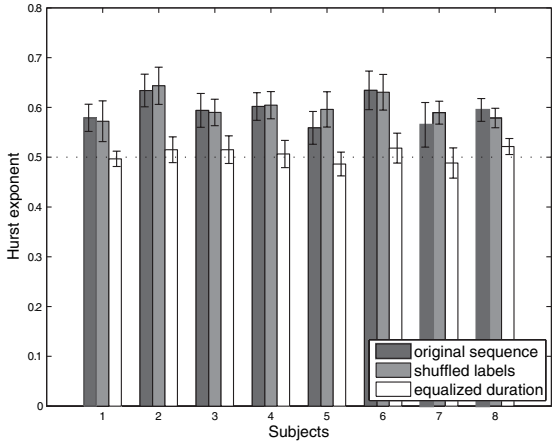


**Fig. 4.** Hurst exponent for the different subjects (data recorded inside the scanner) using original, shuffled, and equalized microstate sequences. The error bars indicate the SD of the estimate over sessions and possible bipartitions of the microstates.

## Conclusions

We uncovered scale-free dynamics of EEG microstates over six dyadic scales covering two orders of magnitude during the awake resting state. This finding provides a compelling explanation of how rapidly changing microstates as measured by EEG are linked to intrinsic brain activity of RSNs as measured by fMRI (71). It also suggests that the brain is a complex system that operates far from homeostatis, which enables it to adapt to incoming information by an ultimate integration of activity at different temporal scales. We hope that this work will stimulate future research to disentangle the basics of cognition and consciousness (72).

## Materials and Methods

**Subjects and Procedure.** Nine healthy right-handed individuals participated for monetary compensation after giving informed consent approved by the University Hospital of Geneva Ethics Committee. None suffered from current or prior neurological or psychiatric impairments or claustrophobia. Mean age of participants was 28.37 y (range 24–33 y).

We first recorded one session of 5 min outside the scanner and then three resting-state sessions of 5 min each inside the MRI scanner. Subjects were instructed to relax (eyes closed) and refrain from falling asleep. We also indicated to them to move as little as possible. Subsequent self-report and inspection of sleep pattern of the EEG led to the exclusion of one subject. The data of eight subjects were subjected to further analysis.

The EEG was recorded from 64 sintered Ag/AgCl ring electrodes mounted in an elastic cap (EasyCaps; Falk Minnow Services) and arranged in an extended 10–10 System. Electrodes were equipped with an additional 5 kΩ in series resistor, and impedances were kept below 15 kΩ. The EEG was acquired with a band pass filter between 0.016 and 250 Hz and digitized at 5 kHz, referenced online to the midline frontal-central electrode (FCz) using a battery-powered MRI-compatible EEG system (BrainAmp MR plus; Brainproducts). The ECG was recorded from a bilateral montage above and below the heart from sintered Ag/AgCl electrodes with an additional 15-kΩ resistor and digitized like the scalp EEG using a BrainAmp ExG MR amplifier. The EEG amplifier along with a rechargeable power pack was placed ~15 cm outside the bore. The amplified and digitized EEG signal was transmitted to the recording computer placed outside the scanner room via fiber optic cables.

**EEG Data Processing.** For the data recorded inside the scanner, the gradient artifacts were removed using a sliding average (73) of 21 averages and subsequently, the EEG was down-sampled to 500 Hz and low-pass filtered with a finite-impulse reponse filter with a bandwidth of 70 Hz. The ballistocardiogram [Bacille Calmette-Guérin (BCG)] artifact was removed by first using a sliding average procedure with 11 averages (74) and then applying independent component analysis (ICA) to remove residual BCG along with oculo-motor components. The so-cleaned EEG was then band-pass filtered between 1 and 40 Hz with a Butterworth IIR filter with a roll-off of 48 dB/octave and further downsampled to 125 Hz.

The data recorded outside the scanner were first down-sampled from 5 kHz to 500 Hz. We used ICA to remove oculo-motor artifacts when necessary and finally, we band-pass filtered the EEG with the same Butterworth IIR filter and further down-sampled it to 125 Hz.

**Microstate Analysis.** We first determined the maxima of the global field power (GFP). Because topography remains stable around peaks of the GFP, they are the best representative of the momentary map topography in terms of signal-to-noise ratio (15). All maps marked as GFP peaks (i.e., the voltage values at all electrodes at that time point) were extracted and submitted to a modified spatial cluster analysis using the atomize-agglomerate hierarchical clustering (AAHC) method (75) to identify the most dominant map topographies (10). The optimal number of template maps was determined by means of a cross-validation criterion (76). We then submitted the template maps identified in every single subject into a second AAHC cluster analysis to identify the dominant clusters across all subjects. Fig. S4 shows the template maps for the different subjects for the recordings. Finally, we computed a spatial correlation between the templates identified at the group level and those identified for each subject in every run. We so labeled each individual map with the group template it best corresponded to, to use the same labels for the subsequent group analysis.

We computed the spatial correlation between the four template maps and the instantaneous EEG (77) using a temporal constraint criterion of 32 ms. We then used these spatial correlation time courses to select the dominant microstate $m(k)\in\{1,2,3,4\}$ at each time instant $k$ and submitted those time series to the fractal analysis.

For the analysis using nonfiltered data recorded outside the scanner, we used spatial correlation between the original nonfiltered EEG (sampled at 500 Hz) and the template maps (derived from the down-sampled and filtered data recorded outside the scanner) and then submitted those time series to fractal analysis. We also temporally permuted the nonfiltered EEG and computed the spatial correlation between the permuted nonfiltered data and the same template maps followed by fractal analysis. Finally, we applied the same filtering as that for the data recorded inside to the permuted data and computed the spatial correlation using the template maps followed by fractal analysis.

**Fractal Analysis.** Monofractal behavior imposes a scaling property on the process $X(t)$ that can be characterized by a single parameter known as the Hurst exponent $H$. Specifically, self-similarity implies that the process $X(t)$ and $\tau^H X(t/\tau)$ are distributionally indistinguishable for all scaling factors $\tau > 0$ (78). The Hurst exponent assesses the degree of temporal dependence; i.e., for $0 < H < 0.5$ the process is considered to have short-range dependency, for $H = 0.5$ increments are uncorrelated, and for $0.5 < H < 1$ long-range dependency is observed.

The wavelet transform analyzes the signal under investigation in terms of dilated and shifted wavelet basis functions $\psi(t/a-k)$. Wavelets also have a number of vanishing moments, which render them insensitive to low-frequency trends. The wavelet coefficient at scale $a$ and position $k$ of a signal $X(t)$ is given by

$$d_X(a,k)=\frac{1}{a}\int X(t)\psi\left(\frac{t}{a}-k\right)dt. \quad [1]$$

Advanced methods for fractal analysis have been based on the continuous wavelet transform; that is, the scale parameter $a$ is (at least conceptually) not discretized, and the traces of the modulus maxima of the wavelet coefficients through scale are characteristic of the fractal signature (79). More recently, the framework of wavelet leaders (80, 81) provides an efficient and numerically robust method based on the discrete wavelet transform, which considers wavelet coefficients only at fixed dyadic scales $a = 2^j$. We denote dyadic scales $a = 2^j$ by the exponent $j$ as a shorthand.

On the basis of the wavelet coefficients, we can compute the structure function associated with a power exponent $q \in \mathbb{Z}$ as

$$S(d_X,j,q)=\frac{1}{n_j}\sum_{k=1}^{n_j}\left|d_X(2^j,k)\right|^q, \quad [2]$$

where $n_j$ is the number of wavelet coefficients available at scale $j$. Wavelet leaders (80) allow us to estimate the structure function in a stable way even for negative powers $q$. For monofractal processes, it has been shown that the structure function derived as such should follow a power law as

$$S(d_X,j,q)=C_q 2^{jqH}, \quad \text{for } q\in\left[q_*^-,q_*^+\right], \quad [3]$$

where $H$ is the Hurst exponent defined before. Monofractality is a very demanding model because a single parameter $H$ characterizes the whole process through scale. Therefore, multifractality is an extended model to describe more complex forms of statistical self-similarity. Specifically, the scaling exponent of the structure function can be generalized as

$$S(d_X,j,q)=C_q 2^{j\zeta(q)}, \quad [4]$$

where $\zeta(q)$ has a concave shape instead of the linear behavior $qH$ observed with monofractality. The characteristic function $\zeta(q)$ is commonly parameterized as a polynomial

$$\zeta(q)=\sum_{p=1}^{\infty}c_p\frac{q^p}{p!}, \quad [5]$$

where the coefficients $c_p$ are termed $p$th degree log-cumulants; $c_1$ corresponds to the convential Hurst exponent $H$. The advantage of the multifractal framework is that monofractal behavior can be asserted by evaluating the higher-degree log-cumulants $c_p$, $p \geq 2$.

To perform fractal analysis of microstate sequences, we need to embed the sequence into a random walk; the procedure is illustrated in Fig. 2. Comparable to self-similar analysis of DNA sequences, we first partition the microstate sequence $m(k)$ into two classes (e.g., $C_1 = \{1,2\}$, $C_2 = \{3,4\}$) and then generate the cumulative sum

$$X(n)=\sum_{k=1}^{n}u(k),$$

where $u(k) = +1$, for $m(k) \in C_1$, and $u(k) = -1$, for $m(k) \in C_2$. The three possible embeddings are considered ($C_1 = \{1,2\}$, $C_1 = \{1,3\}$, and $C_1 = \{1,4\}$). Next, the random walk embedding $X(n)$ is analyzed using Daubechies' orthogonal wavelet transform with five vanishing moments, which means the wavelet coefficients are insensitive to low-frequency trends equivalent to fourth-degree polynomials. The scaling spectrum was analyzed for power exponents $q$ in the range $[-5, 5]$ and log-cumulants up to third degree. We verified the effect of the choice of bipartitioning on the fractal parameters (Fig. S2), using a Wilcoxon rank sum test. The results for the individual subjects (Fig. 4) show the SD over session and possible bipartitions. Statistical significance at the group level (Table S1) is determined using the nonparametric two-sided sign test (82).

**ACKNOWLEDGMENTS.** The Cartool software (http://brainmapping.unige.ch/Cartool.htm) was programmed by Denis Brunet from the Functional Brain Mapping Laboratory, Geneva, Switzerland. Our implementation for the fractal analysis is based on the software made available by the Sisyphe research group at the Ecole Normale Supérieur, Lyon, France. This work was supported in part by the Swiss National Science Foundation (Grants PP00P2-123438 and 310030-132952) and in part by the Center for Biomedical Imaging (CIBM) of the Geneva and Lausanne Universities, École Polytechnique Fédérale de Lausanne, and the Leenaards and Louis-Jeantet foundations.

1. Mesulam MM (1998) From sensation to cognition. *Brain* 121:1013–1052.
2. Seeley WW, Crawford RK, Zhou J, Miller BL, Greicius MD (2009) Neurodegenerative diseases target large-scale human brain networks. *Neuron* 62:42–52.
3. Bressler SL (1995) Large-scale cortical networks and cognition. *Brain Res Brain Res Rev* 20:288–304.
4. Bressler SL, Tognoli E (2006) Operational principles of neurocognitive networks. *Int J Psychophysiol* 60:139–148.
5. Damoiseaux JS, et al. (2006) Consistent resting-state networks across healthy subjects. *Proc Natl Acad Sci USA* 103:13848–13853.
6. Mantini D, Perrucci MG, Del Gratta C, Romani GL, Corbetta M (2007) Electrophysiological signatures of resting state networks in the human brain. *Proc Natl Acad Sci USA* 104: 13170–13175.
7. Lehmann D (1980) *Functional States of the Brain: Their Determinants*, eds Koukkou M, Lehmann D, Angst J (Elsevier, Amsterdam), pp 189–202.
8. Lehmann D, Ozaki H, Pal I (1987) EEG alpha map series: Brain micro-states by space-oriented adaptive segmentation. *Electroencephalogr Clin Neurophysiol* 67:271–288.
9. Mohr C, et al. (2005) Brain state-dependent functional hemispheric specialization in men but not in women. *Cereb Cortex* 15:1451–1458.

10. Britz J, Landis T, Michel CM (2009) Right parietal brain activity precedes perceptual alternation of bistable stimuli. *Cereb Cortex* 19:55–65.
11. Britz J, Pitts MA, Michel CM (2010) Right parietal brain activity precedes perceptual alternation during binocular rivalry. *Hum Brain Mapp*, doi: 10.1002/hbm.21117.
12. Lehmann D, Henggeler B, Koukkou M, Michel CM (1993) Source localization of brain electric field frequency bands during conscious, spontaneous, visual imagery and abstract thought. *Brain Res Cogn Brain Res* 1:203–210.
13. Lehmann D, Pascual-Marqui RD, Strik WK, Koenig T (2010) Core networks for visual-concrete and abstract thought content: A brain electric microstate analysis. *Neuroimage* 49:1073–1079.
14. Lehmann D, Strik WK, Henggeler B, Koenig T, Koukkou M (1998) Brain electric microstates and momentary conscious mind states as building blocks of spontaneous thinking: I. Visual imagery and abstract thoughts. *Int J Psychophysiol* 29:1–11.
15. Koenig T, et al. (2002) Millisecond by millisecond, year by year: Normative EEG microstates and developmental stages. *Neuroimage* 16:41–48.
16. Koenig T, et al. (1999) A deviant EEG brain microstate in acute, neuroleptic-naive schizophrenics at rest. *Eur Arch Psychiatry Clin Neurosci* 249:205–211.
17. Strelets V, et al. (2003) Chronic schizophrenics with positive symptomatology have shortened EEG microstate durations. *Clin Neurophysiol* 114:2043–2051.
18. Strik WK, Dierks T, Becker T, Lehmann D (1995) Larger topographical variance and decreased duration of brain electric microstates in depression. *J Neural Transm* 99:213–222.
19. Dierks T, et al. (1997) EEG-microstates in mild memory impairment and Alzheimer's disease: Possible association with disturbed information processing. *J Neural Transm* 104:483–495.
20. Strik WK, et al. (1997) Decreased EEG microstate duration and anteriorisation of the brain electrical fields in mild and moderate dementia of the Alzheimer type. *Psychiatry Res* 75:183–191.
21. Kinoshita T, et al. (1995) Microstate segmentation of spontaneous multichannel EEG map series under diazepam and sulpiride. *Pharmacopsychiatry* 28:51–55.
22. Kikuchi M, et al. (2007) Native EEG and treatment effects in neuroleptic-naïve schizophrenic patients: Time and frequency domain approaches. *Schizophr Res* 97:163–172.
23. Katayama H, et al. (2007) Classes of multichannel EEG microstates in light and deep hypnotic conditions. *Brain Topogr* 20:7–14.
24. Musso F, Brinkmeyer J, Mobascher A, Warbrick T, Winterer G (2010) Spontaneous brain activity and EEG microstates. A novel EEG/fMRI analysis approach to explore resting-state networks. *Neuroimage* 52:1149–1161.
25. Britz J, Van De Ville D, Michel CM (2010) BOLD correlates of EEG topography reveal rapid resting-state network dynamics. *Neuroimage* 52:1162–1170.
26. Mandelbrot BB (1982) *The Fractal Geometry of Nature* (Freeman, San Francisco).
27. Peng CK, et al. (1992) Long-range correlations in nucleotide sequences. *Nature* 356: 168–170.
28. Ivanov PC, et al. (1999) Multifractality in human heartbeat dynamics. *Nature* 399: 461–465.
29. Goldberger AL, et al. (2002) Fractal dynamics in physiology: Alterations with disease and aging. *Proc Natl Acad Sci USA* 99(Suppl 1):2466–2472.
30. Sporns O, Zwi JD (2004) The small world of the cerebral cortex. *Neuroinformatics* 2: 145–162.
31. Sporns O, Tononi G, Kötter R (2005) The human connectome: A structural description of the human brain. *PLoS Comput Biol* 1:e42.
32. Engel AK, Fries P, Singer W (2001) Dynamic predictions: Oscillations and synchrony in top-down processing. *Nat Rev Neurosci* 2:704–716.
33. Breakspear M, Stam CJ (2005) Dynamics of a neural system with a multiscale architecture. *Philos Trans R Soc Lond B Biol Sci* 360:1051–1074.
34. Achard S, Salvador R, Whitcher B, Suckling J, Bullmore E (2006) A resilient, low-frequency, small-world human brain functional network with highly connected association cortical hubs. *J Neurosci* 26:63–72.
35. Honey CJ, Kötter R, Breakspear M, Sporns O (2007) Network structure of cerebral cortex shapes functional connectivity on multiple time scales. *Proc Natl Acad Sci USA* 104:10240–10245.
36. Bullmore E, et al. (2009) Generic aspects of complexity in brain imaging data and other biological systems. *Neuroimage* 47:1125–1134.
37. Xu N, Xu JH (1988) The fractal dimension of EEG as a physical measure of conscious human brain activities. *Bull Math Biol* 50:559–565.
38. Linkenkaer-Hansen K, Nikouline VV, Palva JM, Ilmoniemi RJ (2001) Long-range temporal correlations and scaling behavior in human brain oscillations. *J Neurosci* 21: 1370–1377.
39. Stam CJ, de Bruin EA (2004) Scale-free dynamics of global functional connectivity in the human brain. *Hum Brain Mapp* 22:97–109.
40. Freeman WJ (2005) A field-theoretic approach to understanding scale-free neocortical dynamics. *Biol Cybern* 92:350–359.
41. Lutzenberger W, Elbert T, Birbaumer N, Ray WJ, Schupp H (1992) The scalp distribution of the fractal dimension of the EEG and its variation with mental tasks. *Brain Topogr* 5:27–34.
42. Pereda E, Gamundi A, Rial R, González J (1998) Non-linear behaviour of human EEG: Fractal exponent versus correlation dimension in awake and sleep stages. *Neurosci Lett* 250:91–94.
43. Carrozzi M, Accardo A, Bouquet F (2004) Analysis of sleep-stage characteristics in full-term newborns by means of spectral and fractal parameters. *Sleep* 27:1384–1393.
44. Weiss B, Clemens Z, Bódizs R, Vágó Z, Halász P (2009) Spatio-temporal analysis of monofractal and multifractal properties of the human sleep EEG. *J Neurosci Methods* 185:116–124.
45. Bullmore ET, Brammer MJ, Alarcon G, Binnie C, Binnie CD (1992) A new technique for fractal analysis applied to human, intracerebrally recorded, ictal electroencephalographic signals. *Neurosci Lett* 146:227–230.
46. Bullmore ET, et al. (1994) Fractal analysis of electroencephalographic signals intracerebrally recorded during 35 epileptic seizures: Evaluation of a new method for synoptic visualisation of ictal events. *Electroencephalogr Clin Neurophysiol* 91: 337–345.
47. Woyshville MJ, Calabrese JR (1994) Quantification of occipital EEG changes in Alzheimer's disease utilizing a new metric: The fractal dimension. *Biol Psychiatry* 35: 381–387.
48. Besthorn C, Sattel H, Geiger-Kabisch C, Zerfass R, Förstl H (1995) Parameters of EEG dimensional complexity in Alzheimer's disease. *Electroencephalogr Clin Neurophysiol* 95:84–89.
49. Bahrami B, Seyedsadjadi R, Babadi B, Noroozian M (2005) Brain complexity increases in mania. *Neuroreport* 16:187–191.
50. Henderson G, et al. (2006) Development and assessment of methods for detecting dementia using the human electroencephalogram. *IEEE Trans Biomed Eng* 53: 1557–1568.
51. Raghavendra BS, Dutt DN, Halahalli HN, John JP (2009) Complexity analysis of EEG in patients with schizophrenia using fractal dimension. *Physiol Meas* 30:795–808.
52. Wackermann J, Lehmann D, Michel CM, Strik WK (1993) Adaptive segmentation of spontaneous EEG map series into spatially defined microstates. *Int J Psychophysiol* 14: 269–283.
53. Lehmann D, et al. (2005) EEG microstate duration and syntax in acute, medication-naive, first-episode schizophrenia: A multi-center study. *Psychiatry Res* 138:141–156.
54. Daubechies I (1992) *Ten Lectures on Wavelets* (Society for Industrial and Applied Mathematics, Philadelphia).
55. Mallat S (2009) *A Wavelet Tour of Signal Processing: The Sparse Way* (Academic, San Diego).
56. Zhan Y, Halliday D, Jiang P, Liu X, Feng J (2006) Detecting time-dependent coherence between non-stationary electrophysiological signals—a combined statistical and time-frequency approach. *J Neurosci Methods* 156:322–332.
57. de Pasquale F, et al. (2010) Temporal dynamics of spontaneous MEG activity in brain networks. *Proc Natl Acad Sci USA* 107:6040–6045.
58. Werner G (2007) Brain dynamics across levels of organization. *J Physiol Paris* 101: 273–279.
59. Scheffer M, et al. (2009) Early-warning signals for critical transitions. *Nature* 461: 53–59.
60. de Arcangelis L, Herrmann HJ (2010) Learning as a phenomenon occurring in a critical state. *Proc Natl Acad Sci USA* 107:3977–3981.
61. Lewis CM, Baldassarre A, Committeri G, Romani GL, Corbetta M (2009) Learning sculpts the spontaneous activity of the resting human brain. *Proc Natl Acad Sci USA* 106:17558–17563.
62. Kitzbichler MG, Smith ML, Christensen SR, Bullmore E (2009) Broadband criticality of human brain network synchronization. *PLoS Comput Biol* 5:e1000314.
63. Lehmann D, Strik WK, Henggeler B, Koenig T, Koukkou M (1998) Brain electric microstates and momentary conscious mind states as building blocks of spontaneous thinking: I. Visual imagery and abstract thoughts. *Int J Psychophysiol* 29:1–11.
64. Lehmann D (1992) *Evolution of Dynamical Structures in Complex Systems*, eds Friedrich R, Wunderlin A (Springer, Berlin), pp 235–248.
65. Changeux JP (1983) *L'Homme Neuronal* (Fayard, Paris).
66. Dehaene S, Kerszberg M, Changeux JP (1998) A neuronal model of a global workspace in effortful cognitive tasks. *Proc Natl Acad Sci USA* 95:14529–14534.
67. Changeux JP, Michel CM (2006) *Microcircuits: The Interface Between Neurons and Global Brain Function*, eds Grillner S, Grabye AM (MIT Press, Cambridge, MA), pp 347–370.
68. Peng CK, Hausdorff JM, Goldberger AL (2000) *Self-Organized Biological Dynamics and Nonlinear Control*, ed Walleczek J (Cambridge Univ Press, Cambridge, UK), pp 66–96.
69. Bak P, Tang C, Wiesenfeld K (1987) Self-organized criticality: An explanation of the 1/f noise. *Phys Rev Lett* 59:381–384.
70. Fingelkurts AA, Fingelkurts AA (2006) Timing in cognition and EEG brain dynamics: Discreteness versus continuity. *Cogn Process* 7:135–162.
71. Raichle ME (2006) Neuroscience. The brain's dark energy. *Science* 314:1249–1250.
72. Koch C (2004) *The Quest for Consciousness* (Roberts, Englewood, CO).
73. Allen PJ, Josephs O, Turner R (2000) A method for removing imaging artifact from continuous EEG recorded during functional MRI. *Neuroimage* 12:230–239.
74. Allen PJ, Polizzi G, Krakow K, Fish DR, Lemieux L (1998) Identification of EEG events in the MR scanner: The problem of pulse artifact and a method for its subtraction. *Neuroimage* 8:229–239.
75. Tibshirani R, Walther G (2005) Cluster validation by prediction strength. *J Comput Graph Stat* 14:511–528.
76. Pascual-Marqui RD, Michel CM, Lehmann D (1995) Segmentation of brain electrical activity into microstates: Model estimation and validation. *IEEE Trans Biomed Eng* 42: 658–665.
77. Murray MM, Brunet D, Michel CM (2008) Topographic ERP analyses: A step-by-step tutorial review. *Brain Topogr* 20:249–264.
78. Samorodnitsky G, Taqqu M (1994) *Stable Non-Gaussian Random Processes* (Chapman & Hall, London).
79. Arneodo A, Grasseau G, Holschneider M (1988) Wavelet transform of multifractals. *Phys Rev Lett* 61:2281–2284.
80. Jaffard S (2004) Wavelet techniques in multifractal analysis. *Proceedings of Symposia in Pure Mathematics*, eds Lapidus M, van Frankenhuijsen M (AMS, Providence, RI), Vol 72, pp 91–152.
81. Wendt H, Abry P, Jaffard S (2007) Bootstrap for empirical multifractal analysis. *IEEE Signal Process Mag* 24:38–48.
82. Hollander M, Wolfe DA (1999) *Nonparametric Statistical Methods* (Wiley, Hoboken, NJ).